274. On the causal inference in magnetosphere / solar wind system during geomagnetic storms.

Manuel Lacal Mirko Piersanti Giuseppe Consolini

University of Trento / University of L'Aquila

Abstract

The Sun, a vital source of light and energy, poses potential hazards through solar storms, particularly during active solar phases occurring every eleven years. These storms can disrupt power grids, radio networks, and satellites if directed toward Earth. In this cases geomagnetic storms can occur. Since these events are typically monitored through the SYM-H geomagnetic index, a comprehensive understanding and accurate modeling of the SYM-H index's dynamics features are essential for investigating about geomagnetic storms. This work aims to study the causal relations between magnetospheric dynamics and external drivers, using a bivariate time series causality analysis, which let us to estimate the normalized information transfer between the variables of the system. Preliminary results show important qualitatively agreements with [1] which used linear correlation analysis.

Research objectives

- **Objective:** investigate the causal relations between magnetospheric dynamics and external drivers during geomagnetic storms

Introduction

Solar storms are emissions of energy and charged particles from the Sun, such as *Coronal Mass Ejection* (CME), and can affect Earth's magnetic field, if directed toward Earth. The magnetosphere can usually shield Earth from solar storms, but sometimes, they can cause saturation of transformers, blackout of power systems, disturbances of international comunications, damage satellites and be responsible for exposing astronauts to abnormal levels of radiation [2].

The energy transferred from a solar storm to Earth's magnetic field is primarily determined by the relative orientation of the interplanetary magnetic field within the CME, the source of the geomagnetic storms [3]. If the magnetic field has a southward component for enough time, the interplanetary plasma can penetrate the magnetosphere, intensifying its current systems. This intensification, particularly of the ring current circulating in the magnetospheric equatorial plane, triggers geomagnetic storms. These events are typically monitored through the *SYM-H* geomagnetic index [4, 5]. Therefore, a comprehensive understanding and accurate modeling of the *SYM-H* index's dynamic features are essential for investigating about geomagnetic storms.

This work aims to study the causal relations between magnetospheric dynamics and external drivers, using a bivariate time series causality analysis, which let us to reconstruct the causal graph of the system, following the methodology outlined by [6]. This method takes as input a linear 2D continuous-time stochastic system for a bivariate time series and provides an estimation of the asymmetric *information transfer* between the system's compoents. As defined by [6], these values are normalized and subjected to statistical significance testing.

This work focuses on finding the most relevant solar wind / magnetosphere coupling functions [1] in terms of the normalized information transfer with respect to *SYM-H*. In detail, in order to study the response time of the magnetosphere to external solar wind drivers, here it is used a delayed version of the net normalized information flow.

Data and Methods

Data

In this study we use solar wind time series from Advanced Composition Explorer (ACE) spacecraft and geomagnetic time series of the low-latitude, retrieved at OMNI website, during periods of 36 geomagnetic storms occured between 1998 and 2018:

- Magnetic field measurements are in GSM reference frame with a temporal resolution of 16 s (ACE),
- Solar wind speed, also in GSM, and proton density with a temporal resolution of 64 s (ACE),
- Geomagnetic index SYM-H with a temporal resolution of 1 min (OMNIWeb).

In the Figure 1, we focus on the north-south component (B_z) of the magnetic field, the solar wind speed, the proton density and the SYM-H index, during a strong geomagnetic storm ($K_{P,max} = 7+$).

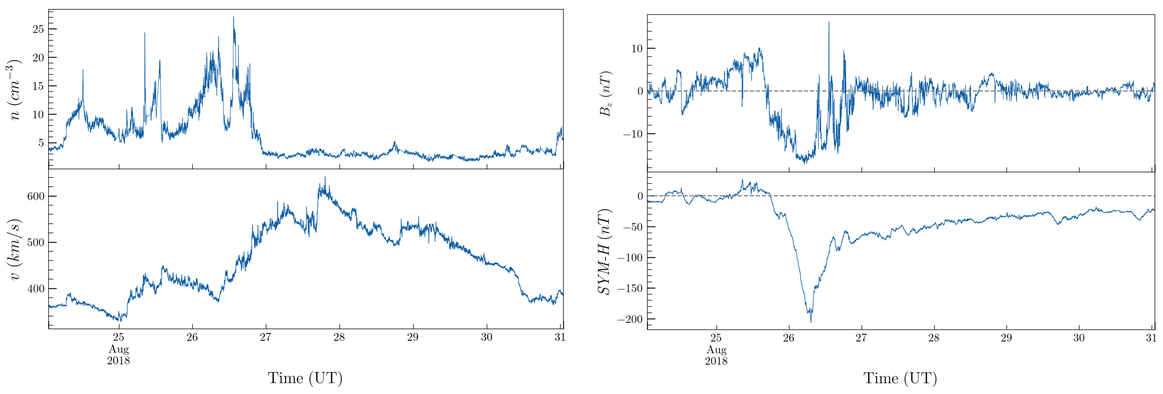

Figure 1. The solar wind speed, v, and the proton density, n (on the left). The north-south component, B_z, and the SYM-H index, for a selected period relative to a geomagnetic storm (on the right).

Following the procedure of [7] the magnetic field and the plasma data are time-shifted from ACE position (L1) to the nose of the bow shock to focus on the response of the magnetosphere to the solar wind, and finally resampled at 1 min.

Methods

Consider a linear 2D continuous-time stochastic system for $\mathbf{X} = (X_1, X_2)$:

$$d\mathbf{X} = \mathbf{f} + \mathbf{A}\mathbf{X}dt + \mathbf{B}d\mathbf{W}, \tag{1}$$

where $\mathbf{f} = (f_1, f_2)$ is a constant vector, $\mathbf{A} = (a_{ij})$ and $\mathbf{B} = (b_{ij})$ (matrix of perturbation amplitudes) are constant matrices, and $\mathbf{W}$ a vector of standard Wiener process. The assumptions are:

- $\mathbf{X} \sim \mathcal{N}(\mu, \mathbf{\Sigma})$, with $\boldsymbol{\mu} = (\mu_1, \mu_2)^T$ and $\mathbf{\Sigma} = (\sigma_{ij})$ being the mean vector and covariance matrix, respectively;
- data is stationary and equal-distanced with time stepsize Δt;
- N is large with respect to Δt;
- $b_{ij} = 0$ if $i \neq j$;
- $\mathbf{F} = \mathbf{f} + \mathbf{A}\mathbf{X}$ and B are differentiable.

Let the transition pdf be $\rho\left(\mathbf{X}_{n+1} \mid \mathbf{X}_n; \boldsymbol{\theta}\right)$, where $\boldsymbol{\theta}$ stands for the vector of parameters to be estimated, so, the log likelihood is

$$\ell_N(\boldsymbol{\theta}) \simeq \sum_{n=1}^{N} \log \rho\left(\mathbf{X}_{n+1} \mid \mathbf{X}_n; \boldsymbol{\theta}\right). \tag{2}$$

Maximizing ℓ_N leads to the maximum-likelihood estimators (mle), which led to the estimator of the information flow, for example from X_2 to X_1:

$$T_{2\to1} = \frac{1}{\det \mathbf{C}} \cdot \sum_{j=1}^{2} \Delta_{2j} C_{j,d1} \cdot \frac{C_{12}}{C_{11}}, \tag{3}$$

where C_{ij} and $C_{i,dj}$ are the sample covariances, and Δ_{ij} are the cofactors of the matrix $\mathbf{C} = (C_{ij})$.

The normalization of (3), following [6], is given by

$$\mathcal{T}_{2\to1} = \frac{T_{2\to1}}{Z_1} \in [-1, 1], \tag{4}$$

where

$$Z_1 = |a_{11}| + |T_{2\to1}| + \frac{1}{2}\frac{b_{11}^2}{|C_{11}|}.$$

The first term represents the contribution of itself, the second part are the information to flows X_1 and the last term is the effect of the noise.

Results and discussion

We start the causal analysis by computing all the solar wind/magnetosphere coupling functions reported in [1], as listed in Table 1.

For each coupling function $Q(t)$, we considered a time-shifted version, i.e., $Q(t+\tau)$, with $\tau \in [1, 200]$ min. We then defined $X(t) = \text{SYM-H}(t)$ (response) and $Y(t) = Q(t+\tau)$ (driver), and computed the *delayed normalized net information flow* $\Delta\mathcal{T}_{Y\leftrightarrow X}(\tau) = |\mathcal{T}_{Y\to X}(\tau)| - |\mathcal{T}_{X\to Y}(\tau)|$. This analysis was conducted for each storm, after which the results were averaged, and the standard deviation of the mean was considered as error. Figure 2 presents the results associated with each of the coupling functions considered. Table 2 ranks the coupling functions with respect to the higher values of $\langle\Delta\mathcal{T}_{Y\leftrightarrow X}(\tau^*)\rangle$, where $\tau^* = \underset{\tau}{\text{argmax}}\left(\langle\Delta\mathcal{T}_{Y\leftrightarrow X}(\tau)\rangle\right)$.

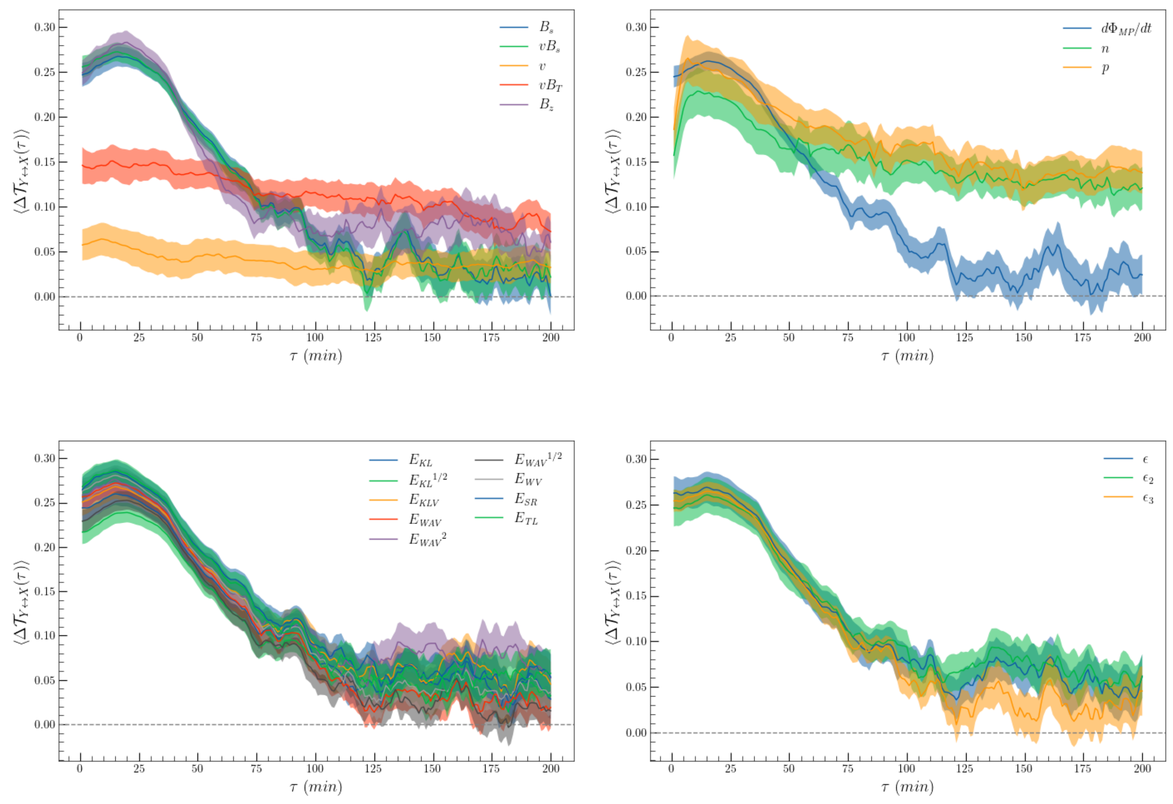

Figure 2. Mean normalized net information flow $\langle\Delta\mathcal{T}_{Y\leftrightarrow X}(\tau)\rangle$ between $Q(t+\tau)$ and SYM-H as a function of τ, for all the coupling function considered (solid line) together with its standard deviation (shaded area).

Our analysis reveals that the functional form of the electric field emerges as the optimal choice. This finding aligns qualitatively with the results presented by [1], which is a reasonable outcome given our use of a linear model (1) in conjunction with linear correlations of [1]. The observed discrepancies may be attributed to the use of different datasets compared to those used by [1]. Notably, our dataset boasts a higher resolution (1 min) as opposed to [1]'s 1-hour resolution.

These findings set the stages for future work in modeling the magnetosphere's response to the solar wind, for example, using differential equations.

Name	$Q(t)$
B_z	B_z
Velocity	v
Density	n
p	$nv^2/2$
B_s	$B_z\,(B_z < 0)$ $0\,(B_z \geq 0)$
Half-wave rectifier	vB_s
ϵ	$vB^2\sin^4(\theta_c/2)$
ϵ_2	$vB_T{}^2\sin^4(\theta_c/2)$
ϵ_3	$vB\sin^4(\theta_c/2)$
Solar wind E-field	vB_T
E_{KL}	$vB\sin^2(\theta_c/2)$
$E_{KL}{}^{1/2}$	$[vB_T\sin^2(\theta_c/2)]^{1/2}$
E_{KLV}	$v^{4/3}B_T\sin^2(\theta_c/2)\,p^{1/6}$
E_{WAV}	$vB_T\sin^4(\theta_c/2)$
$E_{WAV}{}^2$	$[vB_T\sin^4(\theta_c/2)]^2$
$E_{WAV}{}^{1/2}$	$[vB_T\sin^4(\theta_c/2)]^{1/2}$
E_{WV}	$v^{4/3}B_T\sin^4(\theta_c/2)\,p^{1/6}$
E_{SR}	$vB_T\sin^4(\theta_c/2)\,p^{1/2}$
E_{TL}	$n^{1/2}v^2B_T\sin^6(\theta_c/2)$
$d\Phi_{MP}/dt$	$v^{4/3}B_T^{2/3}\sin^{8/3}(\theta_c/2)$

Table 1. Solar wind-magnetosphere coupling functions taken from [1].

$Q(t)$	$\langle\Delta\mathcal{T}_{Y\leftrightarrow X}(\tau^*)\rangle$	τ^* (min)
E_{TL}	0.286 ± 0.012	16
E_{SR}	0.285 ± 0.013	15
B_z	0.283 ± 0.013	20
E_{WV}	0.281 ± 0.011	15
$E_{WAV}{}^2$	0.276 ± 0.013	15
vB_s	0.273 ± 0.011	16
E_{WAV}	0.272 ± 0.011	15
ϵ	0.269 ± 0.017	15
E_{KLV}	0.268 ± 0.014	15
B_s	0.268 ± 0.011	16
p	0.266 ± 0.026	7
ϵ_3	0.264 ± 0.010	15
$d\Phi_{MP}/dt$	0.262 ± 0.011	15
ϵ_2	0.260 ± 0.020	15
E_{KL}	0.260 ± 0.013	15
$E_{WAV}{}^{1/2}$	0.252 ± 0.010	20
$E_{KL}{}^{1/2}$	0.239 ± 0.011	20
n	0.229 ± 0.026	11
vB_T	0.151 ± 0.018	14
v	0.064 ± 0.018	9

Table 2. Solar wind-magnetosphere coupling functions taken from [1].

Conclusions

This study analyzed causal relations between magnetospheric dynamics and solar wind drivers during geomagnetic storms using high-resolution data. Key findings include:

- Electric field-related coupling functions (E_{TL}, E_{SR}) exhibit the highest normalized information transfer, highlighting their significant role in geomagnetic storms.
- Results align with previous studies (e.g., Newell et al., 2007), validating our methodology.

Future work will focus on extending this analysis to differential equations to model the magnetosphere's response to solar wind.

References

[1] P. T. Newell, T. Sotirelis, K. Liou, C.-I. Meng, and F. J. Rich, "A nearly universal solar wind-magnetosphere coupling function inferred from 10 magnetospheric state variables," *Journal of Geophysical Research: Space Physics*, vol. 112, no. A1, 2007. https://doi.org/10.1029/2006JA012015.

[2] O. E. Malandraki and N. B. Crosby, *Solar particle radiation storms forecasting and analysis: The HESPERIA HORIZON 2020 project and beyond*, vol. 444. Springer Nature, 2018. Chap.1. https://doi.org/10.1007/978-3-319-60051-2.

[3] T. Pulkkinen, "Space weather: Terrestrial perspective," *Living Reviews in Solar Physics*, vol. 4, pp. 1–60, 2007. https://doi.org/10.12942/lrsp-2007-1.

[4] J. A. Wanliss and K. M. Showalter, "High-resolution global storm index: Dst versus SYM-H," *Journal of Geophysical Research: Space Physics*, vol. 111, no. A2, 2006. https://doi.org/10.1029/2005JA011034.

[5] B. T. Tsurutani, W. D. Gonzalez, and Y. Kamide, "Magnetic storms," *Surveys in geophysics*, vol. 18, no. 4, pp. 363–383, 1997. https://doi.org/10.1023/A:1006555215463.

[6] X. S. Liang, "Normalized multivariate time series causality analysis and causal graph reconstruction," *Entropy*, vol. 23, no. 6, p. 679, 2021. https://doi.org/10.3390/e23060679.

[7] T. Alberti, G. Consolini, F. Lepreti, M. Laurenza, A. Vecchio, and V. Carbone, "Timescale separation in the solar wind-magnetosphere coupling during St. Patrick's Day storms in 2013 and 2015," *Journal of Geophysical Research: Space Physics*, vol. 122, no. 4, pp. 4266–4283, 2017.

Correspondence to: manuel.lacal@unitn.it